EUROPEAN RESPIRATORY *journal*

FLAGSHIP SCIENTIFIC JOURNAL OF ERS

Early View

Original article

Radiomic Measures from Chest HRCT Associated with Lung Function in Sarcoidosis

Sarah M. Ryan, Tasha E. Fingerlin, Margaret Mroz, Briana Barkes, Nabeel Hamzeh, Lisa A. Maier, Nichole E. Carlson

Please cite this article as: Ryan SM, Fingerlin TE, Mroz M, *et al*. Radiomic Measures from Chest HRCT Associated with Lung Function in Sarcoidosis. *Eur Respir J* 2019; in press (https://doi.org/10.1183/13993003.00371-2019).

TITLE PAGE

1. Title: Radiomic Measures from Chest HRCT Associated with Lung Function in Sarcoidosis
2. Authors: Sarah M. Ryan[1], Tasha E. Fingerlin[1,2,3], Margaret Mroz[4], Briana Barkes[4], Nabeel Hamzeh[5], Lisa A. Maier[4,6,7], Nichole E. Carlson[1]
3. Institutions: [1]Colorado School of Public Health, Department of Biostatistics and Informatics; [2]Colorado School of Public Health, Department of Epidemiology; [3]National Jewish Health, Department of Biomedical Research; [4]National Jewish Health, Department of Medicine; [5]University of Iowa Hospitals and Clinics; [6]University of Colorado, Department of Medicine; [7]Colorado School of Public Health, Department of Environmental and Occupational Health
4. Corresponding Author: Sarah M. Ryan, sarah.m.ryan@ucdenver.edu
5. Summary “take home” message

   Radiomic measures identify pulmonary parenchymal abnormalities in sarcoidosis and are highly associated with lung function, suggesting that radiomics could enhance visual reads and result in improved patient profiling, disease staging and monitoring.

ABSTRACT

Introduction. Pulmonary sarcoidosis is a rare heterogenous lung disease of unknown etiology, with limited treatment options. Phenotyping relies on clinical testing including visual scoring of chest radiographs. Objective radiomic measures from high resolution computed tomography (HRCT) may provide additional information to assess disease status. As the first radiomics analysis in sarcoidosis, we investigate the potential of radiomics as biomarkers for sarcoidosis, by assessing (1) differences in HRCT between sarcoidosis and controls, (2) associations between radiomic measures and spirometry, and (3) trends between Scadding stages.

Methods. Radiomic features were computed on HRCT in three anatomical planes. Linear regression compared global radiomic features between sarcoidosis (N=73) and controls (N=78) and identified associations with spirometry. Spatial differences in associations across the lung were investigated using functional data analysis. A sub-analysis compared radiomic features between Scadding stages.

Results. Global radiomic measures differed significantly between sarcoidosis and control ($p<0.001$ for skewness, kurtosis, fractal dimension and Geary's C), with differences in spatial radiomics most apparent in superior and lateral regions. In sarcoidosis subjects, there were significant associations between radiomic measures and spirometry, with a large association found between Geary's C and forced vital capacity (FVC) ($p=0.008$). Global radiomic measures differed significantly between Scadding stages ($p<0.032$), albeit non-linearly, with stage IV having more extreme radiomic values. Radiomics explained 71.1% of the variability in FVC compared to 51.4% with Scadding staging alone.

Conclusions. Radiomic HRCT measures objectively differentiate disease abnormalities, associate with lung function, and identify trends in Scadding stage, showing promise as quantitative biomarkers for pulmonary sarcoidosis.

INTRODUCTION

Pulmonary sarcoidosis is a rare heterogenous disease of unknown etiology characterized by the formation of granulomas in the lungs, as well as other organs. Compromised lung function is common with pulmonary involvement[1], which can limit daily activities, and frequently indicates the need for therapy to reduce or reverse abnormalities. Spontaneous remission has been quoted to occur in up to two thirds of patients in certain populations[2]. Yet, mortality rates due to respiratory failure are rising in the US[3].

Assessment of chest radiography, in addition to lung function, is used to clinically monitor sarcoidosis, with chest radiographs showing abnormalities in 90% of cases[4]. The Scadding system of staging, based on chest radiographs, is a common visual classification for sarcoidosis, dividing the radiographic manifestations into five stages: stage 0 (no radiograph abnormalities), stage I (bilateral hilar lymphadenopathy, BHL), stage II (pulmonary infiltration with BHL), stage III (pulmonary infiltration without BHL), and stage IV (pulmonary fibrosis with volume loss). Despite the numerical nomenclature, there is no sequential ordering of Scadding stages, and subjects may demonstrate abnormalities in multiple stages at various times. Additional chest radiographic patterns may be observed that are not well characterized by Scadding stage, such as small nodular opacities along the bronchovascular bundle, focal consolidation, consolidation of small nodular opacities (conglomerate masses), ground-glass, and fibrosis, among others[2].

Recently, high-resolution computed tomography (HRCT) scans have been used to characterize pulmonary sarcoidosis manifestations[5–7]. Despite limited standard visual assessment tools for CT sarcoidosis manifestations[8–10], CT findings are still visually characterized, which is time-consuming, dependent on the expertise of the reader, and subject to poor inter-rater reliability[11]. Quantitative assessment of HRCT in sarcoidosis may provide a

more rapid, objective, and sensitive quantification of the various abnormalities that present in sarcoidosis.

Radiomics, an emerging field in which large numbers of quantitative imaging features are computed from medical images, has proved useful for developing quantitative biomarkers in emphysema[12–15]interstitial lung disease[16–18]and lung cancer[19–23]. To our knowledge, radiomic measures have yet to be explored in sarcoidosis. Given the usefulness of radiomics in other diseases, we hypothesize that radiomic features will also prove useful as potential imaging biomarkers for sarcoidosis.

In this paper, we perform an early stage investigation of radiomics as a potential biomarker in sarcoidosis, where early stage references the biomarker study pipeline suggested by Pepe[24]. Our goal is to investigate whether specific radiomic features on lung HRCT differ between sarcoidosis cases and healthy controls (Figure 1 and Table 1). In particular, we compute global and spatially-varying radiomic features, and assess how these measures differentiate sarcoidosis (N=73) from healthy controls (N=78), and between Scadding stages. Lastly, we relate radiomics and lung function to show the potential of radiomics as biomarkers for sarcoidosis.

METHODS

Study Populations and Data Acquisition

Online Data Supplement Section E1 includes a detailed description of the study populations and imaging acquisition. In brief, the sarcoidosis population (N=79) was recruited at National Jewish Health (NJH) as part of the NHLBI funded Genomic Research in Alpha-1 Antitrypsin Deficiency and Sarcoidosis (GRADS) study[25]. A non-smoking, healthy control population (N=108) was obtained from the COPDGene study[26]. Subjects in GRADS were between 18 and 85 years old, had a confirmed diagnosis of sarcoidosis via biopsy or

manifestations consistent with acute sarcoidosis (Lofgren's syndrome)[25]. Subjects in the COPDGene study were between 45 and 80 years old, with no history of lung disease and normal postbronchodilator spirometry[27]. In both GRADS and COPDGene, pulmonary function testing was obtained (PFT, including pre-bronchodilator (BD) forced expiratory volume at one second (FEV1) and forced vital capacity (FVC)) and a chest HRCT ordered according to the same imaging protocol[26], except for a difference in tube current average (GRADS: 180-330 mA varied by BMI; COPDGene: 400 mA); according to Mackin[28], we do not believe the difference in tube current will affect our results. Seventy-three of the GRADS subjects had an HRCT. Only COPDGene subjects scanned on the same machine manufacturer as the GRADS subjects were analyzed in this study (N=78). All subjects provided signed informed consent through either the GRADS or COPDGene studies.

Radiomic Measures

Image data pre-processing and radiomics is described in Online Data Supplement Sections E2 and E3. In brief, lung segmentation and radiomic calculation were performed using the `lungct` R package (https://github.com/ryansar/lungct). Five radiomic measures (skewness, kurtosis, fractal dimension[29], Moran's I[30] and Geary's C[31]) were pre-selected for evaluation in our study based on their statistical properties and success in previous studies for idiopathic pulmonary fibrosis and lung nodules[32,20,33]. The five radiomic measures were computed on every slice for every subject in each of the two lungs and three anatomical planes. To summarize the distribution of the radiomic features obtained for each subject, lung and plane, the median value was computed. Detailed descriptions of each measure along with directional clinical hypotheses for each measure can be found in Figure 1 and Table 1.

Statistical Analysis

A detailed statistical analysis can be found in Online Data Supplement Section E4. Descriptive statistics (e.g. mean and standard deviation for continuous variables; frequencies for categorical variables) were used to summarize demographic, radiomic, and spirometry data (Table 2). Linear regression models were used to test for differences in global radiomic measures between sarcoidosis and healthy controls, adjusted for age, gender, and BMI (Table 3 and Table E1, E2). To evaluate whether disease status (i.e. sarcoidosis vs. control) alters associations between lung function and global radiomic measures, linear regressions were fitted with an interaction between disease group and a global radiomic measure (Figure 2 and Tables E3, E4). In secondary analyses, functional regressions using penalized smoothing splines[34] were fitted to determine whether there was a spatially-varying association between subjects with and without sarcoidosis and a radiomic measure; that is, whether certain regions of the lung were more different between sarcoidosis and control than other regions (Figures 3, 4 and Figures E1, E2).

The above analyses were repeated in sarcoidosis subjects to investigate potential trends in radiomic and lung function measures across Scadding stages (Figure 5 and Figures E3).

Results were considered significant at $p < 0.05$.

RESULTS

For brevity, the results presented here are for the left lung axial orientation, unless otherwise noted. In general, similar patterns were seen for the right lung, and coronal & sagittal anatomical planes (see Online Data Supplement for more information).

Differences in Non-Radiomic Characteristics between Sarcoidosis and Controls and across Scadding Stages in Sarcoidosis.

Table 2 shows the characteristics of the subject population in this study. Compared to controls (N=78), sarcoidosis subjects (N=73) were younger [54.1 (SD 8.6) vs. 64.5 (SD 8.3) years; p<0.001], with a higher BMI [30.1 (SD 7.0) vs. 28.0 (SD 4.8); p=0.029], larger population of white (84.9% vs. 94.1%, p=0.002) and a meaningfully, but not significantly, higher percentage of men (49.3% vs 35.9%; p=0.133). Adjusted for gender, race, ethnicity, age and height, sarcoidosis had significantly lower pre-bronchodilator FEV1 and FVC (p<0.001 for both) compared to controls, but a similar FEV1:FVC ratio (p=0.465).

Subject characteristics were similar across the Scadding stages (Table 2; p>0.05), with differences observed in BMI and the FEV1:FVC ratio (p=0.040 and p<0.001, respectively). Stage IV had the lowest FEV1:FVC ratio, while others had FEV1:FVC ratios within a normal range.

Differences in Global Radiomic Measures were Observed between Sarcoidosis and Controls

The average of the global skewness was positive, but lower in sarcoidosis subjects compared to controls [3.17 (SE 0.09) vs. 3.64 (SE 0.06); p<0.001], as was the global kurtosis [12.7 (SE 0.7) vs. 16.7 (SE 0.6); p<0.001], global fractal dimension [2.404 (SE 0.004) vs. 2.429 (SE 0.003); p<0.001], and global Geary's C [0.212 (SE 0.002) vs. 0.226 (SE 0.002)]; the average global Moran's I [0.702 (SE 0.005) vs. 0.691 (SE 0.004)] was higher in sarcoidosis subjects (p<0.001) (Table 3, and Tables E1 & E2).

Associations were Apparent between Global Radiomic Measures and Lung Function and Differed between Sarcoidosis and Controls

Kurtosis. The relationship between kurtosis and pre-BD FEV1 (Figure 2A) differed between sarcoidosis and control subjects (p=0.032); in sarcoidosis subjects

there was a positive association between kurtosis and FEV1 (β=0.053 L, SE=0.012; p<0.001); however, in controls, there was no significant association between kurtosis and FEV1 (p=0.189). The relationship between kurtosis and FVC and FEV1:FVC was positive (Figure 2B & 2C) and did not differ between sarcoidosis and control subjects (p>0.087).

Geary's C. The association between Geary's C and pre-BD FEV1 (Figure 2D), pre-BD FVC (Figure 2E) and FEV1:FVC (Figure 2F) differed between sarcoidosis and controls (p<0.001, p=0.002, and p<0.001, respectively); in sarcoidosis subjects, there were significant positive associations between Geary's C and FEV1, FVC, and FEV1:FVC (FEV1: β=15.7 L, SE=3.6, p<0.001; FVC: β=21.4 L, SE=4.6, p=0.008; FEV1:FVC: β=2.11 units, SE=0.42, p<0.001); however, in control subjects, there were significant negative associations between Geary's C and FEV1 and FEV1:FVC (FEV1: β=-10.9 L, SE=4.5, p=0.016; FEV1:FVC: β=-1.06 units, SE=0.51, p=0.040).

Differences in Spatial Radiomic Measures were Noted Between Sarcoidosis and Controls

Radiomic measures differed between cases and controls throughout much of the lung across all three planes, as exhibited by separation of confidence bands in Figure 3, and t-statistics greater than 1.96 in Figure 4. Skewness (top panel in Figure 3, yellow in Figure 4) and kurtosis (second row in Figure 3, light green in Figure 4) were significantly lower in sarcoidosis compared to controls, with the largest significant differences observed in the superior and middle sagittal lung regions; smaller, but still significant differences were observed in the coronal plane. Fractal dimension (third row in Figure 3, teal in Figure 4) and Moran's I (fourth row in Figure 3, dark blue in Figure 4) were significantly higher, and Geary's C (bottom panel in

Figure 3, dark purple in Figure 4) significantly lower in the sarcoidosis population, with the most significant differences in the superior and lateral lung regions; there were also large differences in fractal dimension in the coronal plane. See Online Data Supplement Figures E1 and E2 for right lung results.

Radiomic Measures of HRCT Differed According to Scadding Stage Classifications

Global radiomic measures differed when patients were classified by Scadding stage, across all anatomical orientations, with the significant differences driven by Stage IV (Table 3). Not surprisingly, radiomic measures did not follow a sequential increasing or decreasing pattern across Scadding stages. In addition, the various radiomic measures did not follow the same patterns across Scadding stages in terms of which stages have higher (or lower) mean values compared to others. The average of the global skewness, kurtosis and fractal dimension were highest in stage I subjects and lowest in stage IV ($p=0.027$, $p=0.032$, $p<0.001$, respectively). For the global Moran's I, the average was lowest in stage 0 subjects [0.667 (SE 0.013)], and highest in stage IV subjects [0.729 (SE 0.008)] ($p<0.001$). Average Geary's C was highest in stage III subjects [0.229 (SE 0.005)], and lowest in stage IV subjects [0.195 (0.002)] ($p<0.001$).

Importantly, in sarcoidosis subjects, global radiomic measures explained more variation in the lung function measures than Scadding stage measures. For pre-BD FEV1, Scadding stage along with gender, age and BMI explained 44.5% of the variability of pre-BD FEV1, compared to 67.7% with global radiomic measures and gender, age and BMI. Scadding stage along with gender, age and BMI explained 51.4% of the variability in pre-BD FVC, whereas, global radiomic measures along with gender, age and BMI explained 71.1% of the variation in pre-BD FVC. For the FEV1:FVC ratio, Scadding stage, gender, age and BMI explained 26.9%, compared to 40.2% of the variation explained with global radiomic measures, gender, age and BMI.

DISCUSSION

To our knowledge, this is the first radiomics analysis in sarcoidosis. We show the potential of radiomics as biomarkers for sarcoidosis, by (1) detecting differences in HRCT between sarcoidosis and healthy controls, (2) finding associations between radiomic measures and lung function, and (3) identifying trends between Scadding stages. This study can be classified as phase II evidence in the developmental evidence of radiomics as a biomarker for sarcoidosis treatment and disease course prediction[24].

In our findings, global radiomic measures differed significantly between cases and controls in both the left and right lungs in each anatomical plane. The distribution of HUs on CT from subjects with sarcoidosis are more normally distributed (i.e. less skew and kurtosis) as compared to controls. This is due to increased opacification (i.e. whiter areas) on CT scans of sarcoidosis subjects likely caused by parenchymal abnormalities; although it is not clear from our findings which abnormalities are contributing the most. These radiomic findings are consistent with findings via visual assessment that note increased opacification and parenchymal abnormalities on CTs from subjects with sarcoidosis[2]. Moreover, the significant differences in our second-order radiomic features (fractal dimension, Moran's I and Geary's C), show adjacent pixels are more similar (in terms of HUs) on CT scans from subjects with sarcoidosis as compared to controls. This is likely a result of nodule conglomeration and/or fibrosis on CT scans of subjects with sarcoidosis, which is consistent with findings via visual assessment[2]. Furthermore, the spatial radiomic measures displayed significant geographic variation across the lung between cases and controls, with differences most apparent in the superior, mid-to-outer sagittal regions. These spatial findings suggest an upper and lateral lobe predominance of radiographic abnormalities in sarcoidosis, which is consistent with findings on visual assessment[35]. Thus, our radiomic findings are consistent with known visual abnormalities for pulmonary sarcoidosis. It is reassuring that these results support rather than conflict with

visual scoring. A next step in our work will be to assess correlations between visual assessment and radiomic measures and to use the two together to provide an integrative radiologic assessment of pulmonary sarcoidosis.

Global radiomic measures were also significantly associated with spirometry. The association between radiomic measures and lung function was in general stronger among the sarcoidosis population. In sarcoidosis subjects, lower skewness and kurtosis, likely caused by more parenchymal abnormalities, were associated with lower spirometry. Moreover, lower fractal dimension, higher Moran's I and lower Geary's C, likely caused by nodule conglomeration and/or fibrosis, were associated with lower spirometry. It is particularly interesting that there are strong associations between radiomic measures and lung function considering that previous work measuring associations between lung function and visual scoring on CTs from subjects with sarcoidosis has not shown a consistent association[2]. The associations between radiomic measures and spirometry provide further evidence of the potential clinical utility of radiomic analyses in assessment of pulmonary sarcoidosis.

Based on Scadding stage classifications, we found that global radiomics differed significantly in both the left and right lungs in each anatomical plane, with much of the significant differences driven by Scadding stage IV. For skewness, kurtosis, fractal dimension and Geary's C, the most significant pairwise differences were between stage I and IV; for Moran's I, between stage 0 and IV. Not surprisingly, radiomic measures did not follow a sequential increasing or decreasing pattern across Scadding stages. In addition, the various radiomic measures did not follow the same patterns across Scadding stages in terms of which stages have higher (or lower) mean values compared to others. These findings are consistent with our knowledge regarding the non-sequential ordering of Scadding stage[2] and the potential for CT to provide more sensitive and specific information in regards to parenchymal abnormalities in pulmonary sarcoidosis. Specifically, these results suggest that Scadding stage 0 exhibit some type of

abnormality on HRCT. Additionally, these radiomic features appear to be sensitive to parenchymal abnormalities noted in Scadding stage IV, such as fibrosis and/or upper lobe volume loss with hilar retraction. Furthermore, we found that radiomic measures are a better predictor of spirometry than Scadding stage, which is consistent with other studies which note the poor predictive ability of Scadding stage in regards to lung function[36,37].

Further investigation of the utility of radiomic measures as a quantitative biomarker for pulmonary disease, including lung function and other clinical characteristics is warranted, especially given the ability to generate these measures in an automated fashion. A major benefit of a radiomic analysis is the automated computational efficiency and reproducibility, increasing the potential use of these methods in clinical settings. We analyzed 151 segmented scans in approximately three minutes per scan, which is arguably faster than visual assessment. Radiomic algorithms could be programmed into scanners to be available along with visual reads to further enhance a patient's image profile for sarcoidosis staging and disease monitoring.

Our study is not without limitations. This investigation was performed on a modest sample size. Repeating this analysis in a larger sarcoidosis population will be important to verify generalizability and reproducibility. Based on the way the COPDGene cohort was constructed, our control population was only non-smokers. We do not believe that this introduced significant biases given the small proportion of smokers in the sarcoidosis population, and because a sensitivity analysis removing the sarcoidosis patients who smoked showed qualitatively similar results to those we describe above. Although the HRCT scans from both the controls and sarcoidosis were obtained under very similar protocols, we note that a weakness of this study is that the controls and sarcoidosis subjects were scanned on various different Siemens CT machines with different tube currents. This potentially introduces biases due to scanner and protocol differences.

To conclude, our work identifies the usefulness of radiomics on HRCT by efficiently and objectively identifying pulmonary parenchymal abnormalities on subjects with sarcoidosis. We also highlight the significant association between radiomics and lung function, particularly among those with sarcoidosis, suggesting that the radiomic measurements that we evaluated have functional implications. This work shows exciting promise for radiomics as biomarkers for disease in sarcoidosis, which should be further evaluated for application in the clinic and/or research setting. We are hopeful that future research with radiomics on HRCT will result in better understanding about disease progression, classification, and treatment options for subjects with sarcoidosis.

An earlier version of this manuscript was posted to ArXiv in June 2018[38]. Compared to that version, the present manuscript has substantial improvements to its methods, results, and presentation.

REFERENCES

1. Butler MW, Keane MP. Pulmonary sarcoidosis. *Medicine (Baltimore)* 2016;**44**:367–372.

2. Nunes H, Soler P, Valeyre D. Pulmonary sarcoidosis. *Allergy* 2005;**60**:565–582.

3. Swigris JJ, Olson AL, Huie TJ, Fernandez-Perez ER, Solomon J, Sprunger D, Brown KK. Sarcoidosis-related Mortality in the United States from 1988 to 2007. *Am J Respir Crit Care Med* 2011;**183**:1524–1530.

4. Valeyre D, Bernaudin J-F, Uzunhan Y, Kambouchner M, Brillet P-Y, Soussan M, Nunes H. Clinical Presentation of Sarcoidosis and Diagnostic Work-Up. *Semin Respir Crit Care Med* 2014;**35**:336–351.

5. Drent M, De Vries J, Lenters M, Lamers RJS, Rothkranz-Kos S, Wouters EFM, Dieijen-Visser MP van, Verschakelen JA. Sarcoidosis: assessment of disease severity using HRCT. *Eur Radiol* 2003;**13**:2462–2471.

6. Sluimer I, Schilham A, Prokop M, Ginneken B van. Computer analysis of computed tomography scans of the lung: a survey. *IEEE Trans Med Imaging* 2006;**25**:385–405.

7. Keijsers RGM, Heuvel DAF van den, Grutters JC. Imaging the inflammatory activity of sarcoidosis. *Eur Respir J* 2013;**41**:743–751.

8. Nunes H, Uzunhan Y, Gille T, Lamberto C, Valeyre D, Brillet P-Y. Imaging of sarcoidosis of the airways and lung parenchyma and correlation with lung function. *Eur Respir J* 2012;**40**:750–765.

9. Van den Heuvel DA, Jong PA de, Zanen P, Es HW van, Heesewijk JP van, Spee M, Grutters JC. Chest Computed Tomography-Based Scoring of Thoracic Sarcoidosis: Inter-rater Reliability of CT Abnormalities. *Eur Radiol* 2015;**25**:2558–2566.

10. Jacob J, Bartholmai BJ, Rajagopalan S, Kokosi M, Nair A, Karwoski R, Walsh SLF, Wells AU, Hansell DM. Mortality prediction in idiopathic pulmonary fibrosis: evaluation of computer-based CT analysis with conventional severity measures. *Eur Respir J* 2017;**49**:1601011.

11. Wormanns D, Kohl G, Klotz E, Marheine A, Beyer F, Heindel W, Diederich S. Volumetric measurements of pulmonary nodules at multi-row detector CT: in vivo reproducibility. *Eur Radiol* 2004;**14**:86–92.

12. Kumar V, Gu Y, Basu S, Berglund A, Eschrich SA, Schabath MB, Forster K, Aerts HJWL, Dekker A, Fenstermacher D, Goldgof DB, Hall LO, Lambin P, Balagurunathan Y, Gatenby RA, Gillies RJ. Radiomics: the process and the challenges. *Magn Reson Imaging* 2012;**30**:1234–1248.

13. Harmouche R, Ross JC, Diaz AA, Washko GR, Estepar RSJ. A Robust Emphysema Severity Measure Based on Disease Subtypes. *Acad Radiol* 2016;**23**:421–428.

14. Ross JC, Castaldi PJ, Cho MH, Chen J, Chang Y, Dy JG, Silverman EK, Washko GR, Jose Estepar RS. A Bayesian Nonparametric Model for Disease Subtyping: Application to Emphysema Phenotypes. *IEEE Trans Med Imaging* 2017;**36**:343–354.

15. Uppaluri R, Mitsa T, Sonka M, Hoffman EA, McLennan G. Quantification of pulmonary emphysema from lung computed tomography images. *Am J Respir Crit Care Med* 1997;**156**:248–254.

16. Uppaluri R, Hoffman EA, Sonka M, Hunninghake GW, McLennan G. Interstitial lung disease: A quantitative study using the adaptive multiple feature method. *Am J Respir Crit Care Med* 1999;**159**:519–525.

17. Hoffman EA, Reinhardt JM, Sonka M, Simon BA, Guo J, Saba O, Chon D, Samrah S, Shikata H, Tschirren J, Palagyi K, Beck KC, McLennan G. Characterization of the interstitial lung diseases via density-based and texture-based analysis of computed tomography images of lung structure and function. *Acad Radiol* 2003;**10**:1104–1118.

18. Ash SY, Harmouche R, Vallejo DLL, Villalba JA, Ostridge K, Gunville R, Come CE, Onieva Onieva J, Ross JC, Hunninghake GM, El-Chemaly SY, Doyle TJ, Nardelli P, Sanchez-Ferrero GV, Goldberg HJ, Rosas IO, San Jose Estepar R, Washko GR. Densitometric and local histogram based analysis of computed tomography images in patients with idiopathic pulmonary fibrosis. *Respir Res* 2017;**18**.

19. Silva AC, Carvalho PCP, Gattass M. Diagnosis of lung nodule using semivariogram and geometric measures in computerized tomography images. *Comput Methods Programs Biomed* 2005;**79**:31–38.

20. Silva EC da, Silva AC, Paiva AC de, Nunes RA. Diagnosis of lung nodule using Moran's index and Geary's coefficient in computerized tomography images. *Pattern Anal Appl* 2008;**11**:89–99.

21. Wilson R, Devaraj A. Radiomics of pulmonary nodules and lung cancer. *Transl Lung Cancer Res* 2017;**6**:86–91.

22. Lee G, Lee HY, Park H, Schiebler ML, Beek EJR van, Ohno Y, Seo JB, Leung A. Radiomics and its emerging role in lung cancer research, imaging biomarkers and clinical management: State of the art. *Eur J Radiol* 2017;**86**:297–307.

23. Bashir U, Siddique MM, Mclean E, Goh V, Cook GJ. Imaging Heterogeneity in Lung Cancer: Techniques, Applications, and Challenges. *AJR Am J Roentgenol* 2016;**207**:534–543.

24. Pepe MS, Etzioni R, Feng Z, Potter JD, Thompson ML, Thornquist M, Winget M, Yasui Y. Phases of Biomarker Development for Early Detection of Cancer. *JNCI J Natl Cancer Inst* 2001;**93**:1054–1061.

25. Moller DR, Koth LL, Maier LA, Morris A, Drake W, Rossman M, Leader JK, Collman RG, Hamzeh N, Sweiss NJ, Zhang Y, O'Neal S, Senior RM, Becich M, Hochheiser HS, Kaminski N, Wisniewski SR, Gibson KF, GRADS Sarcoidosis Study Group. Rationale and Design of the

Genomic Research in Alpha-1 Antitrypsin Deficiency and Sarcoidosis (GRADS) Study. Sarcoidosis Protocol. *Ann Am Thorac Soc* 2015;**12**:1561–1571.

26. Regan EA, Hokanson JE, Murphy JR, Make B, Lynch DA, Beaty TH, Curran-Everett D, Silverman EK, Crapo JD. Genetic epidemiology of COPD (COPDGene) study design. *COPD* 2010;**7**:32–43.

27. Zach J, Newell J, Schroeder J, Murphy J, Curran-Everett D, Hoffman E, Westgate P, Han M, Silverman E, Crapo J, Lynch D. Quantitative CT of the Lungs and Airways in Healthy Non-smoking Adults. *Invest Radiol* 2012;**47**:596–602.

28. Mackin D, Ger R, Dodge C, Fave X, Chi P-C, Zhang L, Yang J, Bache S, Dodge C, Jones AK, Court L. Effect of tube current on computed tomography radiomic features. *Sci Rep* 2018;**8**:2354.

29. Gneiting T, Ševčíková H, Percival DB. Estimators of Fractal Dimension: Assessing the Roughness of Time Series and Spatial Data. *Stat Sci* 2012;**27**:247–277.

30. Moran PAP. Notes on Continuous Stochastic Phenomena. *Biometrika* 1950;**37**:17–23.

31. Geary RC. The Contiguity Ratio and Statistical Mapping. *Inc Stat* 1954;**5**:115–146.

32. Best AC, Meng J, Lynch AM, Bozic CM, Miller D, Grunwald GK, Lynch DA. Idiopathic Pulmonary Fibrosis: Physiologic Tests, Quantitative CT Indexes, and CT Visual Scores as Predictors of Mortality. *Radiology* 2008;**246**:935–940.

33. Tanabe N, Muro S, Sato S, Oguma T, Sato A, Hirai T. Fractal analysis of low attenuation clusters on computed tomography in chronic obstructive pulmonary disease. *BMC Pulm Med* 2018;**18**:144.

34. Nonparametric Regression and Generalized Linear Models: A roughness penalty approach. CRC Press. https://www.crcpress.com/Nonparametric-Regression-and-Generalized-Linear-Models-A-roughness-penalty/Green-Silverman/p/book/9780412300400 (6 May 2019)

35. III JPL. Computed Tomographic Scanning in Sarcoidosis. *Semin Respir Crit Care Med* 2003;**24**:393–418.

36. Stanojevic S, Wade A, Stocks J, Hankinson J, Coates AL, Pan H, Rosenthal M, Corey M, Lebecque P, Cole TJ. Reference ranges for spirometry across all ages: a new approach. *Am J Respir Crit Care Med* 2008;**177**:253–260.

37. Statement on sarcoidosis. Joint Statement of the American Thoracic Society (ATS), the European Respiratory Society (ERS) and the World Association of Sarcoidosis and Other Granulomatous Disorders (WASOG) adopted by the ATS Board of Directors and by the ERS Executive Committee, February 1999. *Am J Respir Crit Care Med* 1999;**160**:736–755.

38. Ryan SM, Fingerlin T, Hamzeh N, Maier L, Carlson N. An Exploration of Spatial Radiomic Features in Pulmonary Sarcoidosis. *ArXiv180610281 Phys* 2018;

TABLES

Table 1. Description of radiomic features for two-dimensional HRCT slices

Measure and Equation*	Description	Clinical Hypothesis
Skewness $\frac{\frac{1}{n}\sum_{i=1}^{n}(x_i-\bar{x})^3}{\left[\frac{1}{n-1}\sum_{i=1}^{n}(x_i-\bar{x})^2\right]^{3/2}}$	First-order histogram feature that measures the asymmetry of a sample distribution. Positive values indicate right-skew, or a long right tail. Values closer to 0 indicate little or no skew.	Sarcoidosis results in increased opacification (i.e. whiter regions) on HRCT from parenchymal abnormalities. This will alter the properties of the histogram of HU units to appear more normally distributed (i.e. less skew and less kurtosis). Thus, we hypothesize that sarcoidosis subjects will have less skewness and less kurtosis as compared to healthy controls.
Kurtosis $\frac{\frac{1}{n}\sum_{i=1}^{n}(x_i-\bar{x})^4}{\left[\frac{1}{n}\sum_{i=1}^{n}(x_i-\bar{x})^2\right]^2}-3$	First-order histogram feature that measures the tailed-ness of a sample distribution. Positive values indicate infrequent, extreme outliers. Smaller values indicate fewer, less extreme outliers.	
Fractal Dimension $1+median\left[2-\frac{\log V(2)-\log V(1)}{\log 2}\right]$ $V(k)=\frac{\sum_{i=1}^{n}\sum_{j=1}^{n}w_{i,j}(k)\lvert x_i-x_j\rvert}{\sum_{i=1}^{n}\sum_{j=1}^{n}w_{i,j}(k)}$	Second-order texture feature that measures the self-similarity of pixels in space, or the image roughness[29]. On a two-dimensional plane, it ranges from 2 to 3, with lower values indicative of adjacent pixels appearing more similar (i.e. more smoothness).	Sarcoidosis involves the formation of micronodules in the lung that may conglomerate as disease worsens, and/or fibrosis may develop. Conglomeration and fibrosis are both represented by adjacent pixels of higher opacification on HRCT (i.e. more smoothness). Thus, we hypothesize that sarcoidosis subjects will have lower fractal dimension, higher Moran's I and lower Geary's
Moran's I $\frac{n\sum_{i=1}^{n}\sum_{j=1}^{n}w_{i,j}(x_i-\bar{x})(x_j-\bar{x})}{\sum_{i=1}^{n}\sum_{j=1}^{n}w_{i,j}(1)\sum_{i=1}^{n}(x_i-\bar{x})^2}$	Second-order spatial feature that measures global spatial autocorrelation, or similarity of pixels in space[30]. It ranges approximately from -1 to 1, with values around zero indicative of no	

	spatial autocorrelation and higher values indicative of positive spatial autocorrelation, or adjacent pixels appearing more similar.	C as compared to healthy controls.
Geary's C $\frac{n\sum_{i=1}^{n}\sum_{j=1}^{n}w_{i,j}(x_i-x_j)^2}{\sum_{i=1}^{n}\sum_{j=1}^{n}w_{i,j}(1)\sum_{i=1}^{n}(x_i-\bar{x})^2}$	Second-order spatial feature that measures local spatial autocorrelation[31]. Geary's C, ranging from 0 to 2, is inversely proportional to Moran's I, with values close to zero indicating strong positive spatial autocorrelation, or adjacent pixels appearing more similar.	

***** x_i is the HU intensity at a single pixel, i; n is the total number of pixels and $\bar{x}$ is the mean HU from a lung-masked HRCT slice; $w_{i,j}(k)$ is an indicator function for whether the distance between pixels i and j is k units

Table 2. Differences in subject characteristics by case and control status and Scadding stage. Categorical variables are summarized by the frequency (%); continuous variables are summarized by mean (standard deviation). P-values for lung function measures (pre-BD FEV1, FVC, and the ratio) are adjusted for gender, age, race, ethnicity, and height.

	Control (N = 78)	**Sarcoidosis** (N = 73)	**P-value**	**Stage 0** (N = 9)	**Stage I** (N = 8)	**Stage II** (N = 28)	**Stage III** (N = 11)	**Stage IV** (N = 17)	**P-value**
Male (%)	28 (35.9)	36 (49.3)	0.133	2 (22.2%)	3 (37.5%)	14 (50.0%)	7 (63.6%)	10 (58.8%)	0.329
White (%)	**77 (98.7)**	**62 (84.9)**	**0.002**	7 (77.8%)	8 (100.0%)	24 (85.7%)	11 (100.0%)	12 (70.6%)	0.166
Age (years)	**64.51 (8.32)**	**54.14 (8.64)**	**<0.001**	51.44 (7.19)	52.27 (13.79)	53.76 (9.31)	56.93 (6.81)	55.28 (6.24)	0.612

BMI	**27.97 (4.76)**	**30.12 (6.95)**	**0.029**	**36.68 (7.20)**	**29.80 (5.99)**	**28.55 (5.72)**	**30.28 (8.74)**	**29.27 (6.58)**	**0.040**
Pre-BD FEV1 (L)	**2.76 (0.71)**	**2.81 (0.95)**	**<0.001**	2.86 (0.85)	2.98 (1.07)	2.85 (1.05)	3.02 (0.80)	2.39 (0.82)	0.055
Pre-BD FVC (L)	**3.61 (0.90)**	**3.72 (1.20)**	**<0.001**	3.45 (1.03)	3.69 (1.31)	3.87 (1.40)	3.92 (1.06)	3.43 (0.95)	0.140
FEV1:FVC ratio	0.77 (0.05)	0.75 (0.09)	0.465	**0.83 (0.03)**	**0.81 (0.08)**	**0.74 (0.08)**	**0.78 (0.06)**	**0.68 (0.10)**	**<0.001**

Table 3. Differences in global radiomic features between cases and controls and by Scadding stage in the left lung, axial plane. Values are summarized by mean (standard errors). P-values are adjusted for gender, age, and BMI. For right lung and coronal and sagittal results, see Online Data Supplement Table E1 and E2.

	Control (N = 78)	**Sarcoidosis** (N = 73)	**P-value**	**Stage 0** (N = 9)	**Stage I** (N = 8)	**Stage II** (N = 28)	**Stage III** (N = 11)	**Stage IV** (N = 17)	**P-value**
Skewness	3.642 (0.060)	3.166 (0.085)	<0.001	3.009 (0.131)	3.491 (0.198)	3.309 (0.150)	3.373 (0.187)	2.727 (0.172)	0.027
Kurtosis	16.653 (0.600)	12.732 (0.688)	<0.001	10.879 (1.102)	15.052 (2.003)	14.084 (1.259)	14.248 (1.741)	9.413 (1.066)	0.032
Fractal D	2.429 (0.003)	2.404 (0.004)	<0.001	2.434 (0.011)	2.437 (0.006)	2.397 (0.004)	2.421 (0.005)	2.374 (0.008)	<0.001
Moran's I	0.691 (0.004)	0.702 (0.005)	0.047	0.667 (0.013)	0.668 (0.013)	0.715 (0.005)	0.680 (0.007)	0.729 (0.008)	<0.001
Geary's C	0.226 (0.002)	0.212 (0.002)	<0.001	0.226 (0.006)	0.227 (0.005)	0.208 (0.003)	0.229 (0.005)	0.195 (0.002)	<0.001

LEGENDS FOR ILLUSTRATIONS

Figure 1. Representative HRCT scans from subjects representative of HRCT abnormalities, including no abnormalities (S1), mosaic attenuation/honeycombing (S2), nodules (S3), and fibrosis (S4). In general, a two-dimensional HRCT slice from a healthy subject (S1) appears to have mostly healthy lung tissue, with the occasional blood vessel or airway on the slice. Conversely, the HRCT slices from subject with sarcoidosis (S2-S4) have increased opacification and parenchymal abnormalities apparent, shown by the whiter areas on the CT scan. These parenchymal abnormalities on the CT scan for subjects S2-S4 alter the appearance of the Hounsfield unit (HU) histogram, resulting in less skewness and less kurtosis ("peaked") densities, as compared to the healthy subject, S1. Further, the spatial radiomic measures also differ, with sarcoidosis subjects having smaller fractal dimension and Geary's C, and larger Moran's I, as compared to the healthy subject.

Figure 2. Association between lung function and global radiomic features by disease status, adjusted for gender, age, and BMI. P-values on subfigures test for significant associations between lung function and global radiomic features for both sarcoidosis (blue lines) and healthy controls (green lines). Shaded bars represent 95% confidence bands, predicted for a female subject, with a mean age of 59.5 years and mean BMI of 29.0; points represent raw data values per subject, colored by disease group. The global radiomic features are calculated on the left lung, axial orientation. For the right lung, and other orientations, see Online Data Supplement Tables E2 and E3.

Figure 3. Mean radiomic features throughout the lung for sarcoidosis and healthy controls. Shaded bars represent 95% confidence bands; individual lines represent raw radiomic features throughout the lung per individual, colored by disease group. Results are shown for the left lung and all orientations. For right lung results, see Online Data Supplement Figure E1.

Figure 4. Effect size of the absolute difference in radiomic features throughout the lung between sarcoidosis and healthy control subjects, adjusted for gender, age, and BMI. Assuming a normal approximation, values above 1.96 represent statistically significant differences at a significance level of 0.05. Results are shown for the left lung. For right lung results, see Online Data Supplement Figure E2.

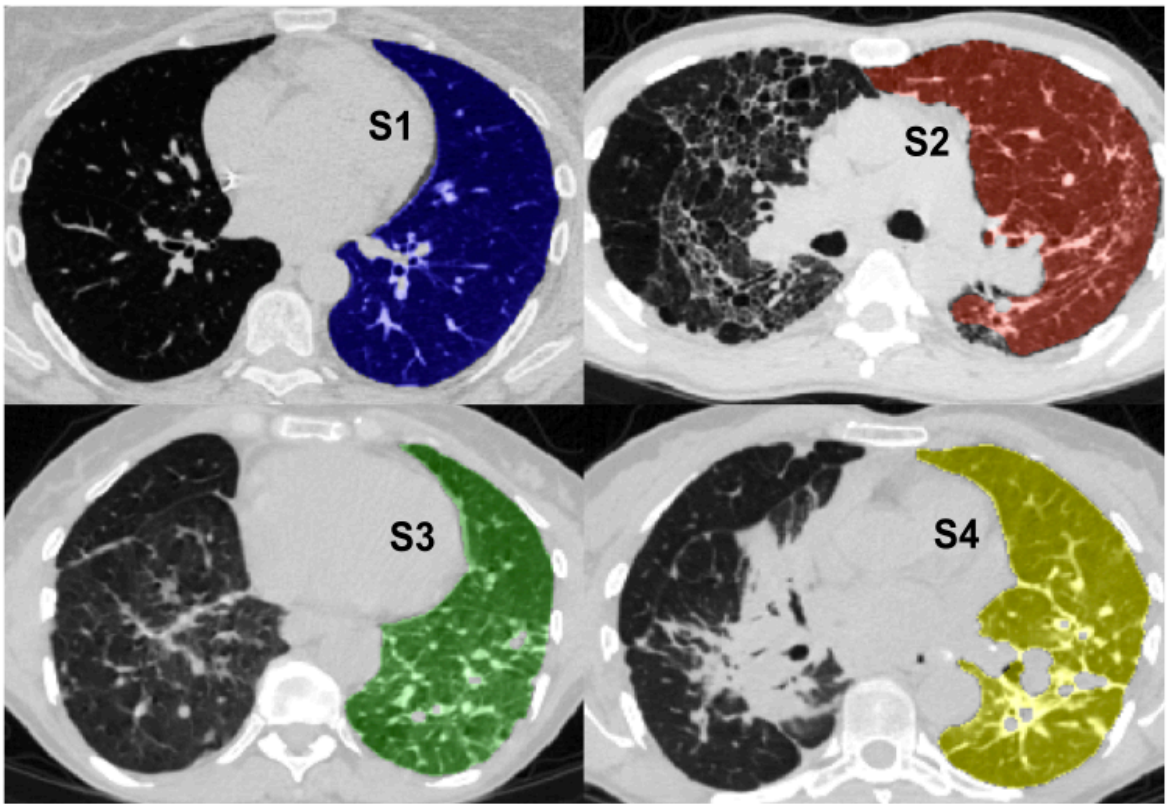
S1
S2
S3
S4

(A)

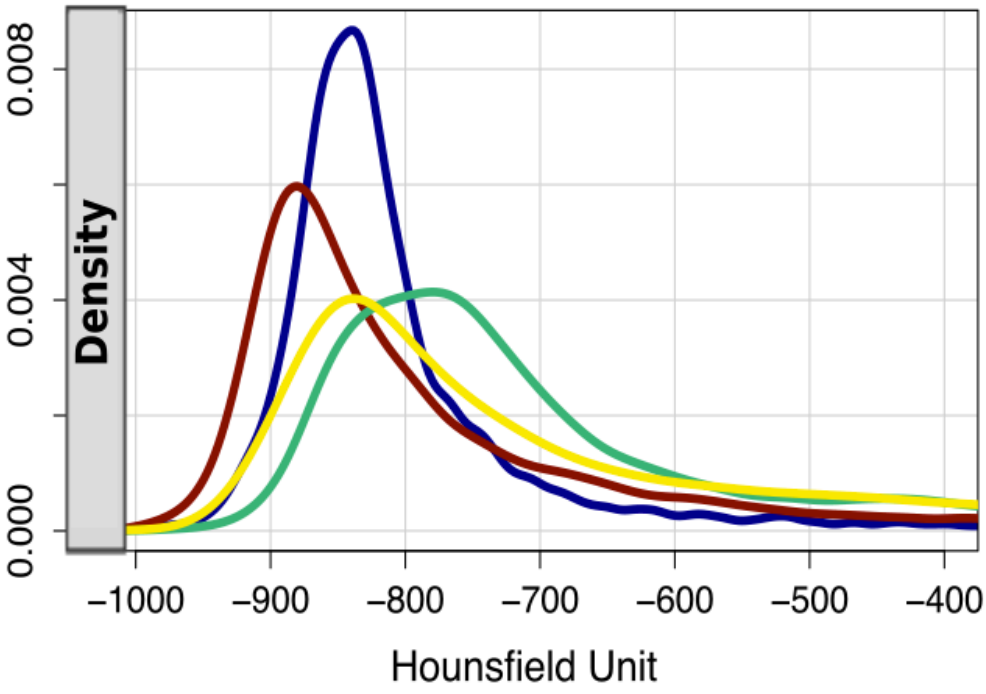
Density
0.000
0.004
0.008
−1000
−900
−800
−700
−600
−500
−400
Hounsfield Unit

(B)

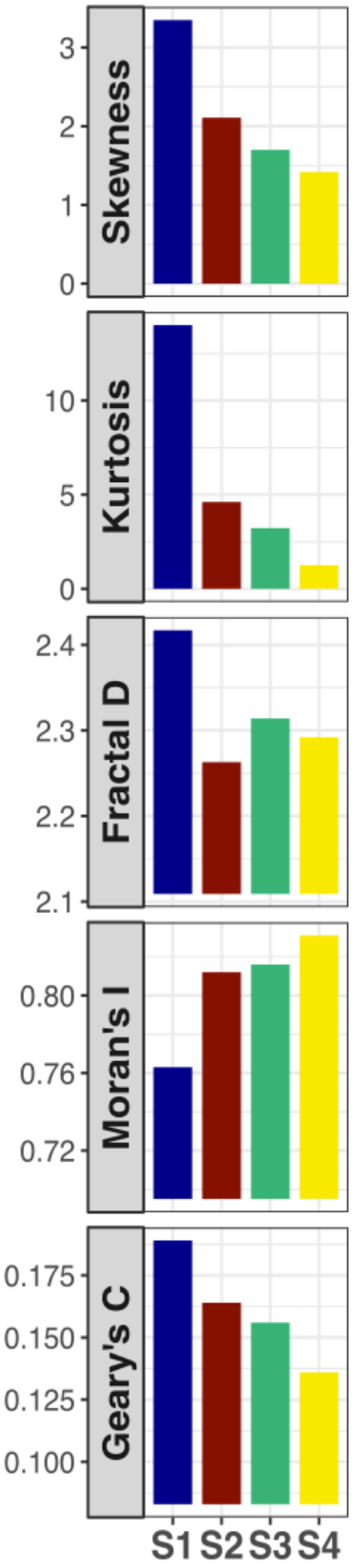
Skewness
0
1
2
3
Kurtosis
0
5
10
Fractal D
2.1
2.2
2.3
2.4
Moran's I
0.72
0.76
0.80
Geary's C
0.100
0.125
0.150
0.175
S1 S2 S3 S4

(C)

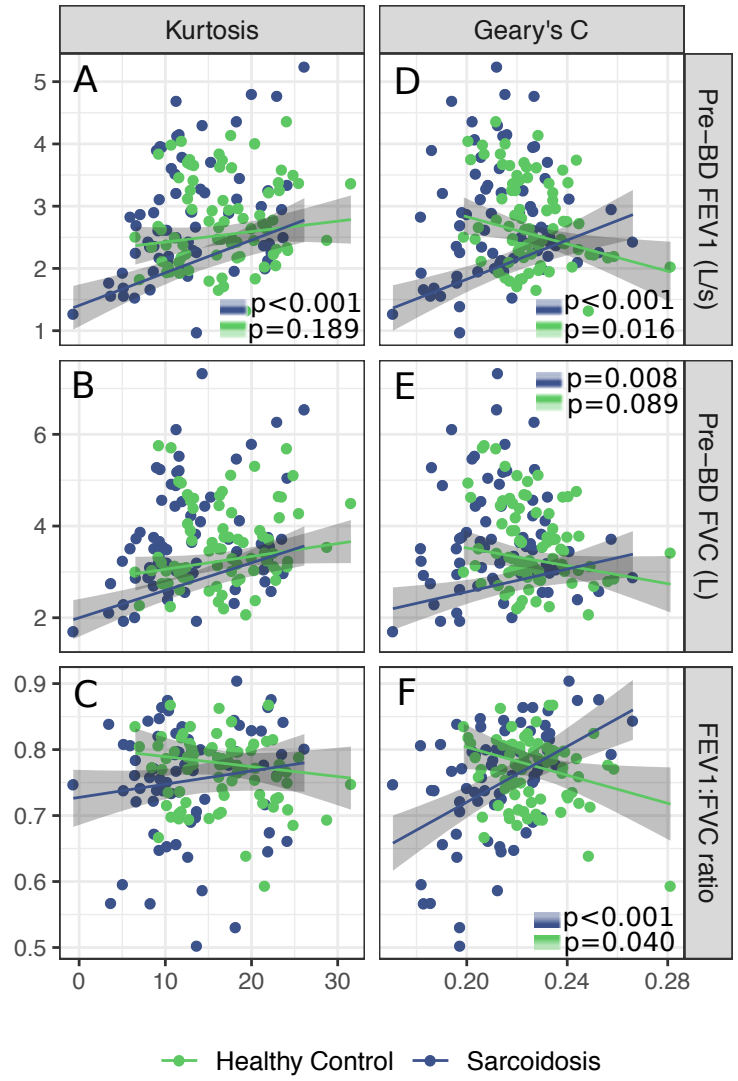
Kurtosis
Geary's C
A
D
B
E
C
F
Pre−BD FEV1 (L/s)
Pre−BD FVC (L)
FEV1:FVC ratio
p<0.001
p=0.189
p<0.001
p=0.016
p=0.008
p=0.089
p<0.001
p=0.040
5
4
3
2
1
6
4
2
0.9
0.8
0.7
0.6
0.5
0
10
20
30
0.20
0.24
0.28
Healthy Control
Sarcoidosis

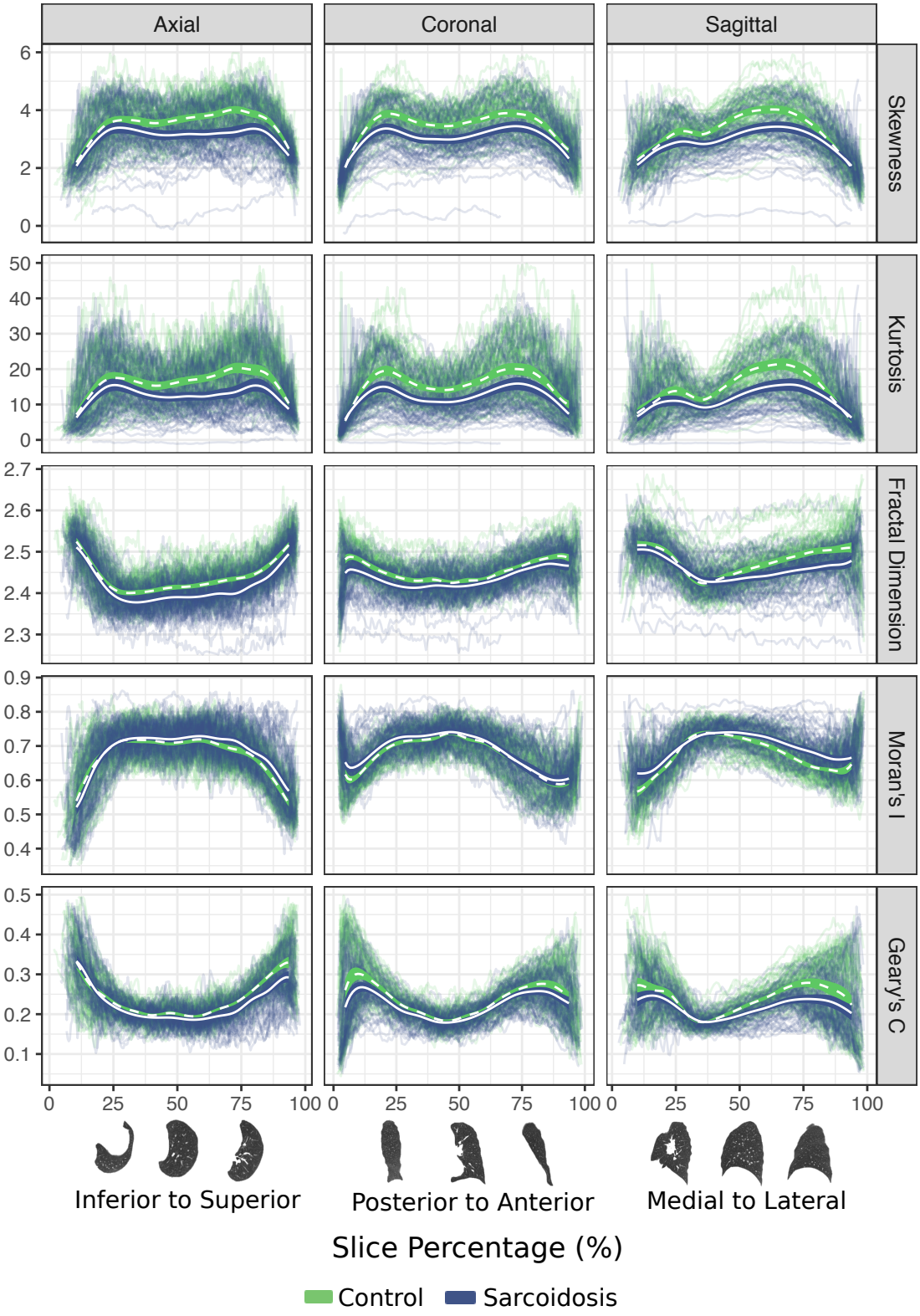
Axial
Coronal
Sagittal
Skewness
Kurtosis
Fractal Dimension
Moran's I
Geary's C
Inferior to Superior
Posterior to Anterior
Medial to Lateral
Slice Percentage (%)
Control
Sarcoidosis

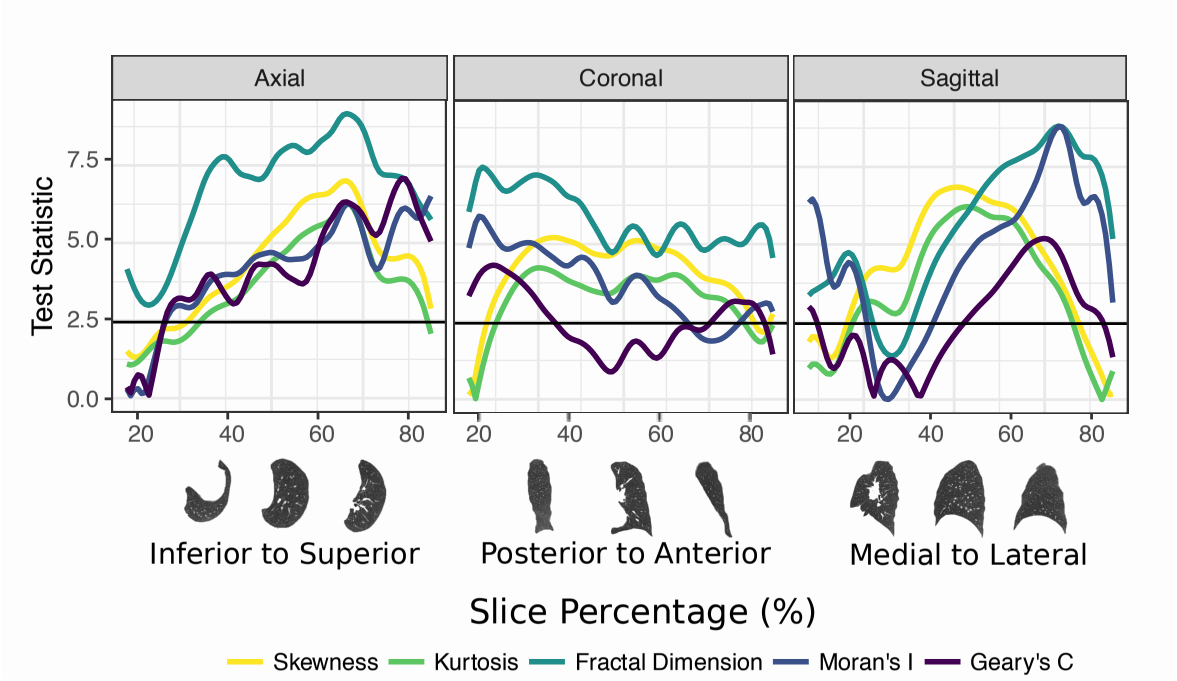
Axial
Coronal
Sagittal
Test Statistic
7.5
5.0
2.5
0.0
20
40
60
80
Inferior to Superior
Posterior to Anterior
Medial to Lateral
Slice Percentage (%)
Skewness
Kurtosis
Fractal Dimension
Moran's I
Geary's C

ONLINE DATA SUPPLEMENT:

Radiomic Measures from Chest HRCT Associated with Lung Function in Sarcoidosis

Sarah M. Ryan, Tasha E. Fingerlin, Margaret Mroz, Briana Barkes, Nabeel Hamzeh, Lisa A. Maier, Nichole E. Carlson

Section E1. Study Populations and Data Acquisition

The sarcoidosis population used in this study was recruited at National Jewish Health (NJH) as part of the NHLBI funded Genomic Research in Alpha-1 Antitrypsin Deficiency and Sarcoidosis (GRADS) study. The GRADS study is a multi-center, observational cohort exploring the role of the microbiome and genome in subjects with Alpha-1 Antitrypsin Deficiency and/or Sarcoidosis[1]. Subjects were eligible for GRADS if they were between the ages of 18 and 85 years, had a confirmed diagnosis of sarcoidosis via biopsy or manifestations consistent with acute sarcoidosis (Lofgren's syndrome), met one of the nine study phenotypes and provided signed informed consent. As part of GRADS, uniform clinical data was obtained including pulmonary function testing (PFT, including pre-bronchodilator (BD) forced expiratory volume at one second (FEV1), forced vital capacity (FVC), and diffusing capacity of the lungs for carbon monoxide (DLCO)), a chest radiograph (for Scadding staging classification), and a research chest HRCT based on the COPDGene protocol[2]. Of 79 GRADS sarcoidosis subjects enrolled at NJH, N=73 subjects with a HRCT usable for quantitative analysis were used in this study. Research chest HRCTs used in this study were acquired using Siemens SOMATOM Definition (N=22) or Siemens SOMATOM Definition AS+ (N=51), with the participants in the supine position during breath holding at end inspiration, and the following parameters: 120 kVp, effective tube current average 180-

330 mA (varied by BMI), 500 msec exposure time, standard B35f kernel, 0.75 mm thickness, and computed interval of 0.5 mm[1].

A non-smoking, healthy control population was obtained from the COPDGene study. COPDGene is a cross-sectional prospective cohort exploring epidemiological and genetic characteristics in smokers with and without chronic obstructive pulmonary disease[3]. A total of 108 healthy nonsmokers were recruited for COPDGene that were between the ages of 45 and 80 years, with no history of lung disease and normal postbronchodilator spirometry[2]. As part of COPDGene, uniform clinical data was obtained including PFT (spirometry and lung volumes) and a research chest HRCT. As DLCO was not collected in COPDGene, it was not used as an outcome in this study. Of 108 COPDGene non-smoking healthy controls, N=78 subjects were included in the present study who had a HRCT acquired using Siemens SOMATOM Definition (N=45), Siemens SOMATOM Definition Flash (N=25), Siemens SOMATOM Definition AS+ (N=6) or Siemens SOMATOM Sensation 64 (N=2). These HRCT had the same parameters as GRADS, except for a tube current average of 400 mA; according to Mackin[4], we do not believe that this difference in tube current affected our radiomic results.

Section E2. Data-Processing

Each CT scan had the same axial slice thickness (0.750mm) and interval (0.500mm); however, since a 512x512 image matrix was used for the reconstruction, the spacing in the coronal and sagittal planes were dependent on the size of the subject. To remove spacing variability across subjects and anatomical planes, all scans were resampled to 1x1x1 mm^3 spacing. A thresholding- and region-based segmentation technique, as implemented in the `lungct` R package, was used to segment the left and right lung from the resampled scans. CT scans were further thresholded at HU<0 to remove non-lung tissue found on the boundaries of the masked CT. Masked CT slices with less than 2,000 pixels (approximately

5% or less of the masked slice) were discarded due to small image size and unstable estimates; this resulted in the removal of approximately 15% of slices per person.

Section E3. Radiomic Measures

Radiomics can be divided into first and second order measures. First order measures quantify features of the distribution of the Hounsfield unit (HU) pixel values, such as the mean, median, standard deviation, skewness and kurtosis, among others[5]. Second order measures quantify spatial smoothness or associations between adjacent pixels. Examples include grey-level co-occurrence matrices (GLCMs), grey-level run-length matrices (GLRLMs), fractal dimension, Moran's I and Geary's C, among others[5]. Typical radiomic analyses investigate a large number of radiomic features by using a validation procedure, whereby a subset of the data is used to select important radiomic features, and an additional subset of the data is used to evaluate the selected radiomic features[6]. However, this approach requires a large amount of data[7]. Given our moderate sample size (N=151) and to avoid the problem of false positive findings, we have pre-selected five radiomic features that we hypothesize will be useful to differentiate sarcoidosis and control groups.

From the first-order measures, we selected skewness and kurtosis as both measure the non-normality of the distribution which we observe in lung CTs (Figure 1); additionally, both have been shown to be successful for idiopathic pulmonary fibrosis[8], a disease which results in increased opacification on CT scans, similar to sarcoidosis. Since sarcoidosis results in increased opacification (i.e. whiter regions) on HRCT from parenchymal abnormalities (such as micronodules, conglomerate masses, fibrosis and other radiographic patterns), we hypothesized that there would be less skewness and less kurtosis in sarcoidosis subjects as compared to controls; that is, we hypothesize that the increased opacification on the CT scans from sarcoidosis subjects will alter the HU distribution to appear more normally distributed (Figure 1; Table 1).

From the second-order measures, we pre-selected fractal dimension[9], Moran's I[10] and Geary's C[11] as all measure the spatial smoothness of the data, where smoothness is defined as adjacent pixels appearing more similar, which we observe in lung CTs (Figure 1); further, these spatial summaries have shown to be very useful in detecting lung nodules[12,13]. Lower values of fractal dimension and Geary's C, and higher values of Moran's I are indicative of more smoothness. Since sarcoidosis involves the formation of micronodules in the lung that begin to conglomerate as disease worsens and/or fibrosis may develop, we hypothesized that there would be lower fractal dimension, lower Geary's C, and higher Moran's I in sarcoidosis subjects as compared to controls, since the aggregation of nodules (conglomerate masses) will result in adjacent pixels appearing more similar on a CT scan (Figure 1; Table 1).

Fractal dimension was estimated using the line transect madogram estimator for spatial data (27). Moran's I and Geary's C were estimated using an eight-nearest neighbor adjacency matrix. Mathematical representations of these measures can be found in Table 1. All measures were calculated using the `lungct` R package.

Section E4. Statistical Analysis

Demographics. Descriptive statistics (e.g. mean and standard deviation for continuous variables; frequency tables for categorical variables) were used to summarize demographic and spirometry data. To test for an association between disease group and gender, a Chi-square test was used. To test for an association between disease group and race (white/non-white), a Fisher's exact test was used, due to small cell sample sizes. Linear regression models were used to test for differences in means for all continuous variables between sarcoidosis and healthy controls, and between Scadding stages. Continuous variables include age at consent, BMI, pre-BD FEV1, pre-BD FVC, and FEV1:FVC.

Differences in Global Radiomics between Sarcoidosis and Controls. Each radiomic measure was computed on every third slice for every subject in each of the two lungs and

three anatomical planes. To arrive at a single "global" value, the median value across each subject, lung and orientation were computed. Descriptive statistics (e.g. means and standard deviations) were used to summarize the global radiomic measures between disease groups. Linear regression models were used to test for differences in global radiomic measures between sarcoidosis and healthy controls, adjusted for age, gender, and BMI.

Associations between Global Radiomic Measures and Lung Function. To evaluate the difference in disease (i.e. sarcoidosis vs. control) on the association between lung function and global radiomic measures, linear regression was used with an interaction between disease group and global radiomic measures. When the effect of disease group was significant, the association between global radiomic measure and lung function is reported (estimates, standard errors, and p-values) separately by the specific disease; otherwise, the interaction was removed, and the association is reported over all participants.

Differences in Spatial Radiomics between Sarcoidosis and Controls. We also analyzed the curve of radiomic measures throughout the lung that results from the computation of radiomic measures on each slice in both the right and left lung in each of the three anatomical orientations. Functional regression was used to determine whether there is a spatially-varying association between subjects with and without sarcoidosis on each radiomic measure; that is, whether certain regions of the lung were more different between sarcoidosis and control than other regions. We used penalized smoothing splines for our functional data analysis. The optimal degrees of freedom for the penalized smoothing spline was determined using the corrected Akaike Information Criteria (cAIC)[14]. The functional regression was adjusted for gender, age, and BMI. Standard errors and 95% confidence intervals were obtained from 1000 bootstrapped samples. The t-statistic was computed using the absolute value of the difference between sarcoidosis and healthy controls divided by the standard error at each slice percentage.

Comparisons between Scadding Stage. In sarcoidosis subjects, linear regression models were used to test for differences in global radiomic measures between Scadding stages, adjusted for age, gender, and BMI. If a significant difference was found in Scadding stage, pairwise comparisons were performed, with significance defined as $p<0.005$ for multiple comparisons (10 different combinations of pairwise differences between Scadding stages). Linear regression models were also used to estimate the amount of variance in lung function explained (i.e. adjusted r-squared) by Scadding stage versus a combination of global radiomic measures. Step-wise regression based on AIC was used to determine which combination of global radiomic measures resulted in best model fit. Finally, functional regression using penalized smoothing splines were used to summarize radiomic measures throughout the lung between Scadding stages. Due to small sample sizes and low power, only mean estimates by Scadding stage are reported.

Analyses were independently performed for radiomic measures of skewness, kurtosis, fractal dimension, Moran's I, and Geary's C. All analyses were performed in Rstudio v1.0.136. Results were considered significant at a $p < 0.05$.

REFERENCES

1. Moller DR, Koth LL, Maier LA, Morris A, Drake W, Rossman M, Leader JK, Collman RG, Hamzeh N, Sweiss NJ, Zhang Y, O'Neal S, Senior RM, Becich M, Hochheiser HS, Kaminski N, Wisniewski SR, Gibson KF, GRADS Sarcoidosis Study Group. Rationale and Design of the Genomic Research in Alpha-1 Antitrypsin Deficiency and Sarcoidosis (GRADS) Study. Sarcoidosis Protocol. *Ann Am Thorac Soc* 2015;**12**:1561–1571.

2. Zach J, Newell J, Schroeder J, Murphy J, Curran-Everett D, Hoffman E, Westgate P, Han M, Silverman E, Crapo J, Lynch D. Quantitative CT of the Lungs and Airways in Healthy Non-smoking Adults. *Invest Radiol* 2012;**47**:596–602.

3. Regan EA, Hokanson JE, Murphy JR, Make B, Lynch DA, Beaty TH, Curran-Everett D, Silverman EK, Crapo JD. Genetic epidemiology of COPD (COPDGene) study design. *COPD* 2010;**7**:32–43.

4. Mackin D, Ger R, Dodge C, Fave X, Chi P-C, Zhang L, Yang J, Bache S, Dodge C, Jones AK, Court L. Effect of tube current on computed tomography radiomic features. *Sci Rep* 2018;**8**:2354.

5. Lee G, Lee HY, Park H, Schiebler ML, Beek EJR van, Ohno Y, Seo JB, Leung A. Radiomics and its emerging role in lung cancer research, imaging biomarkers and clinical management: State of the art. *Eur J Radiol* 2017;**86**:297–307.

6. Aerts HJWL, Velazquez ER, Leijenaar RTH, Parmar C, Grossmann P, Carvalho S, Cavalho S, Bussink J, Monshouwer R, Haibe-Kains B, Rietveld D, Hoebers F, Rietbergen MM, Leemans CR, Dekker A, Quackenbush J, Gillies RJ, Lambin P. Decoding tumour phenotype by noninvasive imaging using a quantitative radiomics approach. *Nat Commun* 2014;**5**:4006.

7. Gillies RJ, Kinahan PE, Hricak H. Radiomics: Images Are More than Pictures, They Are Data. *Radiology* 2015;**278**:563–577.

8. Best AC, Meng J, Lynch AM, Bozic CM, Miller D, Grunwald GK, Lynch DA. Idiopathic Pulmonary Fibrosis: Physiologic Tests, Quantitative CT Indexes, and CT Visual Scores as Predictors of Mortality. *Radiology* 2008;**246**:935–940.

9. Gneiting T, Ševčíková H, Percival DB. Estimators of Fractal Dimension: Assessing the Roughness of Time Series and Spatial Data. *Stat Sci* 2012;**27**:247–277.

10. Moran PAP. Notes on Continuous Stochastic Phenomena. *Biometrika* 1950;**37**:17–23.

11. Geary RC. The Contiguity Ratio and Statistical Mapping. *Inc Stat* 1954;**5**:115–146.

12. Silva EC da, Silva AC, Paiva AC de, Nunes RA. Diagnosis of lung nodule using Moran's index and Geary's coefficient in computerized tomography images. *Pattern Anal Appl* 2008;**11**:89–99.

13. Tanabe N, Muro S, Sato S, Oguma T, Sato A, Hirai T. Fractal analysis of low attenuation clusters on computed tomography in chronic obstructive pulmonary disease. *BMC Pulm Med* 2018;**18**:144.

14. Hurvich CM, Tsai C-L. The Impact of Model Selection on Inference in Linear Regression. *Am Stat* 1990;**44**:214–217.

TABLES

Table E1. Differences in global radiomic features between pulmonary sarcoidosis and Scadding stage. P-values are adjusted for gender, age, and BMI. Global radiomic features are calculated from global values across the **left** lung. Values are summarized by mean (standard error). Fractal D = fractal dimension.

		Control	Sarcoidosis	P-value	Stage 0	Stage I	Stage II	Stage III	Stage IV	P-value
		(N = 78)	(N = 73)		(N = 9)	(N = 8)	(N = 28)	(N = 11)	(N = 17)	
Axial	Skewness	3.642 (0.060)	3.166 (0.085)	<0.001	3.009 (0.131)	3.491 (0.198)	3.309 (0.150)	3.373 (0.187)	2.727 (0.172)	0.027
	Kurtosis	16.653 (0.600)	12.732 (0.688)	<0.001	10.879 (1.102)	15.052 (2.003)	14.084 (1.259)	14.248 (1.741)	9.413 (1.066)	0.032
	Fractal D	2.429 (0.003)	2.404 (0.004)	<0.001	2.434 (0.011)	2.437 (0.006)	2.397 (0.004)	2.421 (0.005)	2.374 (0.008)	<0.001
	Moran's I	0.691 (0.004)	0.702 (0.005)	0.047	0.667 (0.013)	0.668 (0.013)	0.715 (0.005)	0.680 (0.007)	0.729 (0.008)	<0.001
	Geary's C	0.226 (0.002)	0.212 (0.002)	<0.001	0.226 (0.006)	0.227 (0.005)	0.208 (0.003)	0.229 (0.005)	0.195 (0.002)	<0.001
Coronal	Skewness	3.576 (0.058)	3.115 (0.082)	<0.001	2.945 (0.120)	3.441 (0.194)	3.261 (0.146)	3.337 (0.176)	2.668 (0.166)	0.016
	Kurtosis	16.133 (0.588)	12.349 (0.677)	<0.001	10.335 (1.045)	14.433 (1.903)	13.739 (1.285)	13.955 (1.649)	9.106 (0.958)	0.03
	Fractal D	2.450 (0.003)	2.434 (0.004)	<0.001	2.458 (0.009)	2.460 (0.007)	2.428 (0.004)	2.453 (0.006)	2.404 (0.009)	<0.001
	Moran's I	0.688 (0.004)	0.700 (0.004)	0.01	0.666 (0.012)	0.674 (0.012)	0.711 (0.005)	0.673 (0.008)	0.729 (0.008)	<0.001

	Geary's C	0.235 (0.003)	0.220 (0.003)	<0.001	0.232 (0.009)	0.229 (0.006)	0.219 (0.005)	0.239 (0.006)	0.199 (0.005)	<0.001
Sagittal	Skewness	3.360 (0.054)	2.986 (0.076)	<0.001	2.843 (0.122)	3.272 (0.161)	3.120 (0.129)	3.201 (0.155)	2.567 (0.169)	0.014
	Kurtosis	14.626 (0.567)	11.605 (0.650)	<0.001	9.768 (1.057)	13.578 (1.842)	12.968 (1.188)	13.377 (1.665)	8.257 (0.944)	0.017
	Fractal D	2.478 (0.004)	2.454 (0.005)	<0.001	2.491 (0.015)	2.479 (0.007)	2.449 (0.006)	2.470 (0.008)	2.420 (0.012)	<0.001
	Moran's I	0.684 (0.003)	0.705 (0.004)	<0.001	0.671 (0.010)	0.676 (0.010)	0.715 (0.004)	0.682 (0.005)	0.736 (0.009)	<0.001
	Geary's C	0.239 (0.004)	0.214 (0.004)	<0.001	0.227 (0.009)	0.222 (0.007)	0.215 (0.006)	0.233 (0.010)	0.191 (0.005)	0.002

Table E2. Differences in global radiomic features between pulmonary sarcoidosis and Scadding stage. P-values are adjusted for gender, age, and BMI. Global radiomic features are calculated from global values across the **right** lung. Values are summarized by mean (standard error). Fractal D = fractal dimension.

		Control	**Sarcoidosis**	**P-value**	**Stage 0**	**Stage I**	**Stage II**	**Stage III**	**Stage IV**	**P-value**
		N = 78	N = 73		N = 9	N = 8	N = 28	N = 11	N = 17	
Axial	**Skewness**	3.725 (0.060)	3.181 (0.077)	<0.001	3.150 (0.127)	3.611 (0.200)	3.263 (0.139)	3.435 (0.182)	2.695 (0.114)	0.002
	Kurtosis	17.432 (0.600)	12.839 (0.673)	<0.001	12.007 (1.060)	16.197 (2.091)	13.644 (1.193)	14.888 (1.754)	9.046 (0.933)	0.007
	Fractal D	2.433 (0.003)	2.406 (0.004)	<0.001	2.437 (0.011)	2.439 (0.006)	2.396 (0.004)	2.423 (0.006)	2.380 (0.007)	<0.001

	Moran's I	0.685 (0.004)	0.701 (0.005)	0.003	0.661 (0.015)	0.665 (0.011)	0.715 (0.006)	0.682 (0.008)	0.730 (0.006)	<0.001
	Geary's C	0.232 (0.002)	0.214 (0.002)	<0.001	0.230 (0.006)	0.232 (0.005)	0.209 (0.003)	0.230 (0.005)	0.194 (0.003)	<0.001
Coronal	**Skewness**	3.700 (0.055)	3.172 (0.075)	<0.001	3.103 (0.117)	3.532 (0.198)	3.247 (0.139)	3.433 (0.158)	2.747 (0.123)	0.009
	Kurtosis	17.110 (0.552)	12.770 (0.656)	<0.001	11.591 (0.991)	15.398 (1.984)	13.736 (1.221)	14.590 (1.471)	9.390 (1.023)	0.022
	Fractal D	2.452 (0.003)	2.435 (0.004)	<0.001	2.463 (0.011)	2.459 (0.006)	2.425 (0.004)	2.453 (0.007)	2.411 (0.007)	<0.001
	Moran's I	0.684 (0.003)	0.699 (0.005)	0.001	0.659 (0.013)	0.670 (0.012)	0.712 (0.005)	0.674 (0.009)	0.727 (0.008)	<0.001
	Geary's C	0.238 (0.002)	0.220 (0.003)	<0.001	0.236 (0.006)	0.233 (0.006)	0.217 (0.005)	0.236 (0.006)	0.199 (0.005)	<0.001
Sagittal	**Skewness**	3.449 (0.054)	2.998 (0.069)	<0.001	2.915 (0.120)	3.360 (0.174)	3.092 (0.123)	3.209 (0.157)	2.578 (0.109)	0.003
	Kurtosis	15.261 (0.561)	11.404 (0.613)	<0.001	10.422 (1.102)	14.025 (1.974)	12.450 (1.084)	13.150 (1.604)	7.837 (0.756)	0.006
	Fractal D	2.483 (0.004)	2.457 (0.005)	<0.001	2.500 (0.015)	2.485 (0.008)	2.447 (0.005)	2.474 (0.009)	2.426 (0.009)	<0.001
	Moran's I	0.675 (0.003)	0.701 (0.005)	<0.001	0.658 (0.012)	0.657 (0.009)	0.712 (0.005)	0.681 (0.008)	0.738 (0.007)	<0.001
	Geary's C	0.246 (0.004)	0.221 (0.004)	<0.001	0.239 (0.010)	0.236 (0.008)	0.222 (0.006)	0.233 (0.007)	0.193 (0.006)	<0.001

Table E3. Effect of disease group on the association between lung function and global radiomic features from the left lung, adjusted for gender, age, and BMI. FEV1 = pre-bronchodilator forced expiratory volume at one second. FVC = pre-bronchodilator forced vital capacity. FractalD = fractal dimension.

Position	Outcome	Variable	P-value of difference	Effect of Sarcoidosis	Effect of Control	Effect of both groups	Adjusted R-sq
Axial	FEV1	Skewness	0.056	--	--	0.353 SE=0.078 p<0.001	0.549
Axial	FEV1	Kurtosis	0.032	0.053 SE=0.012 p<0.001	0.017 SE=0.013 p=0.189	--	0.548
Axial	FEV1	FractalD	0.001	9.251 SE=2.217 p<0.001	-1.762 SE=2.846 p=0.537	--	0.54
Axial	FEV1	Moran's I	0.011	-3.681 SE=1.949 p=0.061	3.220 SE=1.895 p=0.091	--	0.504
Axial	FEV1	Geary's C	<0.001	15.711 SE=3.629 p<0.001	-10.928 SE=4.475 p=0.016	--	0.561
Axial	FVC	Skewness	0.127	--	--	0.428 SE=0.094 p<0.001	0.593
Axial	FVC	Kurtosis	0.113	--	--	0.045 SE=0.011 p<0.001	0.585
Axial	FVC	FractalD	0.014	8.566 SE=2.749 p=0.002	-1.850 SE=3.529 p=0.601	--	0.564
Axial	FVC	Moran's I	0.007	-3.166 SE=2.343 p=0.179	5.696 SE=2.279 p=0.014	--	0.557
Axial	FVC	Geary's C	0.002	12.440 SE=4.603	-9.735 SE=5.676	--	0.564

				p=0.008	p=0.089		
Axial	FEV1:FVC	Skewness	0.171	--	--	0.007 SE=0.010 p=0.478	0.057
Axial	FEV1:FVC	Kurtosis	0.087	--	--	0.000 SE=0.001 p=0.712	0.054
Axial	FEV1:FVC	FractalD	0.016	0.879 SE=0.264 p=0.001	-0.097 SE=0.339 p=0.776	--	0.121
Axial	FEV1:FVC	Moran's I	0.381	--	--	-0.418 SE=0.160 p=0.010	0.097
Axial	FEV1:FVC	Geary's C	<0.001	2.114 SE=0.415 p<0.001	-1.063 SE=0.512 p=0.040	--	0.221
Coronal	FEV1	Skewness	0.042	0.497 SE=0.094 p<0.001	0.180 SE=0.130 p=0.167	--	0.569
Coronal	FEV1	Kurtosis	0.023	0.057 SE=0.012 p<0.001	0.018 SE=0.013 p=0.158	--	0.557
Coronal	FEV1	FractalD	<0.001	11.147 SE=2.157 p<0.001	-1.625 SE=2.782 p=0.560	--	0.567
Coronal	FEV1	Moran's I	<0.001	-6.190 SE=2.054 p=0.003	4.347 SE=2.184 p=0.049	--	0.527
Coronal	FEV1	Geary's C	<0.001	12.526 SE=2.631 p<0.001	-1.913 SE=2.809 p=0.497	--	0.556
Coronal	FVC	Skewness	0.127	--	--	0.470 SE=0.096 p<0.001	0.602
Coronal	FVC	Kurtosis	0.106	--	--	0.049 SE=0.011 p<0.001	0.591
Coronal	FVC	FractalD	0.002	10.551	-2.479	--	0.581

				SE=2.703 p<0.001	SE=3.486 p=0.478		
Coronal	FVC	Moran's I	0.001	-4.481 SE=2.500 p=0.075	7.507 SE=2.659 p=0.005	--	0.568
Coronal	FVC	Geary's C	0.043	9.190 SE=3.353 p=0.007	-0.366 SE=3.580 p=0.919	--	0.555
Coronal	FEV1:FVC	Skewness	0.108	--	--	0.009 SE=0.010 p=0.369	0.059
Coronal	FEV1:FVC	Kurtosis	0.063	--	--	0.001 SE=0.001 p=0.647	0.055
Coronal	FEV1:FVC	FractalD	0.034	0.968 SE=0.263 p<0.001	0.109 SE=0.339 p=0.748	--	0.131
Coronal	FEV1:FVC	Moran's I	0.069	--	--	-0.686 SE=0.179 p<0.001	0.142
Coronal	FEV1:FVC	Geary's C	<0.001	1.627 SE=0.298 p<0.001	-0.430 SE=0.318 p=0.178	--	0.23
Sagittal	FEV1	Skewness	0.042	0.510 SE=0.104 p<0.001	0.166 SE=0.139 p=0.235	--	0.558
Sagittal	FEV1	Kurtosis	0.027	0.056 SE=0.012 p<0.001	0.017 SE=0.013 p=0.218	--	0.548
Sagittal	FEV1	FractalD	<0.001	9.363 SE=1.743 p<0.001	0.332 SE=2.033 p=0.870	--	0.571
Sagittal	FEV1	Moran's I	<0.001	-8.043 SE=2.123 p<0.001	5.048 SE=2.741 p=0.068	--	0.541
Sagittal	FEV1	Geary's C	<0.001	10.366 SE=2.209 p<0.001	0.083 SE=2.005 p=0.967	--	0.551

Sagittal	FVC	Skewness	0.115	--	--	0.478 SE=0.105 p<0.001	0.593
Sagittal	FVC	Kurtosis	0.13	--	--	0.048 SE=0.012 p<0.001	0.585
Sagittal	FVC	FractalD	0.009	8.971 SE=2.192 p<0.001	0.970 SE=2.556 p=0.705	--	0.581
Sagittal	FVC	Moran's I	<0.001	-6.323 SE=2.613 p=0.017	8.582 SE=3.374 p=0.012	--	0.571
Sagittal	FVC	Geary's C	0.102	--	--	4.670 SE=1.962 p=0.019	0.552
Sagittal	FEV1:FVC	Skewness	0.124	--	--	0.006 SE=0.011 p=0.553	0.056
Sagittal	FEV1:FVC	Kurtosis	0.047	0.002 SE=0.002 p=0.162	-0.002 SE=0.002 p=0.195	--	0.073
Sagittal	FEV1:FVC	FractalD	0.004	0.781 SE=0.213 p<0.001	-0.071 SE=0.248 p=0.776	--	0.136
Sagittal	FEV1:FVC	Moran's I	0.035	-1.180 SE=0.243 p<0.001	-0.364 SE=0.313 p=0.248	--	0.188
Sagittal	FEV1:FVC	Geary's C	<0.001	1.334 SE=0.248 p<0.001	-0.405 SE=0.225 p=0.075	--	0.232

Table E4. Effect of disease group on the association between lung function and global radiomic features from the right lung, adjusted for gender, age, and BMI. FEV1 = pre-bronchodilator forced expiratory volume at one second. FVC = pre-bronchodilator forced vital capacity. Fractal D = fractal dimension.

Position	Outcome	Variable	P-value of difference	Effect of Sarcoidosis p-value	Effect of Control P-value	Effect of both groups	Adjusted R-sq
Axial	FEV1	Skewness	0.006	0.593 SE=0.099 p<0.001	0.170 SE=0.122 p=0.168	--	0.588
Axial	FEV1	Kurtosis	0.007	0.063 SE=0.012 p<0.001	0.018 SE=0.012 p=0.150	--	0.571
Axial	FEV1	FractalD	0.001	10.610 SE=2.344 p<0.001	-1.299 SE=3.046 p=0.671	--	0.549
Axial	FEV1	Moran's I	0.008	-4.250 SE=1.907 p=0.027	2.609 SE=1.781 p=0.145	--	0.506
Axial	FEV1	Geary's C	<0.001	15.915 SE=3.301 p<0.001	-7.303 SE=4.122 p=0.079	--	0.564
Axial	FVC	Skewness	0.041	0.645 SE=0.122 p<0.001	0.261 SE=0.151 p=0.086	--	0.613
Axial	FVC	Kurtosis	0.054	--	--	0.050 SE=0.011 p<0.001	0.594
Axial	FVC	FractalD	0.019	8.776 SE=2.947 p=0.003	-1.810 SE=3.830 p=0.637	--	0.559
Axial	FVC	Moran's I	0.012	-3.342 SE=2.310 p=0.150	4.590 SE=2.158 p=0.035	--	0.553
Axial	FVC	Geary's C	0.01	12.459 SE=4.216	-4.887 SE=5.265	--	0.561

				p=0.004	p=0.355		
Axial	FEV1:FVC	Skewness	0.026	0.032 SE=0.013 p=0.013	-0.012 SE=0.016 p=0.458	--	0.094
Axial	FEV1:FVC	Kurtosis	0.021	0.003 SE=0.001 p=0.028	-0.001 SE=0.002 p=0.337	--	0.088
Axial	FEV1:FVC	FractalD	0.007	1.211 SE=0.275 p<0.001	0.065 SE=0.357 p=0.856	--	0.164
Axial	FEV1:FVC	Moran's I	0.143	--	--	-0.426 SE=0.153 p=0.006	0.102
Axial	FEV1:FVC	Geary's C	<0.001	2.044 SE=0.374 p<0.001	-1.043 SE=0.468 p=0.027	--	0.241
Coronal	FEV1	Skewness	0.012	0.618 SE=0.101 p<0.001	0.207 SE=0.134 p=0.126	--	0.593
Coronal	FEV1	Kurtosis	0.01	0.065 SE=0.012 p<0.001	0.021 SE=0.013 p=0.128	--	0.575
Coronal	FEV1	FractalD	<0.001	12.481 SE=2.379 p<0.001	-0.556 SE=3.040 p=0.855	--	0.569
Coronal	FEV1	Moran's I	0.003	-5.142 SE=2.053 p=0.013	3.794 SE=2.289 p=0.100	--	0.514
Coronal	FEV1	Geary's C	0.002	10.426 SE=2.783 p<0.001	-3.417 SE=3.521 p=0.333	--	0.532
Coronal	FVC	Skewness	0.054	--	--	0.568 SE=0.103 p<0.001	0.616
Coronal	FVC	Kurtosis	0.056	--	--	0.057 SE=0.011 p<0.001	0.604
Coronal	FVC	FractalD	0.004	11.165	-1.611	--	0.576

				SE=3.002 p<0.001	SE=3.836 p=0.675		
Coronal	FVC	Moran's I	0.004	-3.360 SE=2.488 p=0.179	7.136 SE=2.774 p=0.011	--	0.559
Coronal	FVC	Geary's C	0.109	--	--	3.899 SE=2.863 p=0.175	0.54
Coronal	FEV1:FVC	Skewness	0.075	--	--	0.012 SE=0.011 p=0.260	0.062
Coronal	FEV1:FVC	Kurtosis	0.06	--	--	0.001 SE=0.001 p=0.539	0.056
Coronal	FEV1:FVC	FractalD	0.025	1.248 SE=0.285 p<0.001	0.295 SE=0.364 p=0.419	--	0.161
Coronal	FEV1:FVC	Moran's I	0.225	--	--	-0.716 SE=0.181 p<0.001	0.148
Coronal	FEV1:FVC	Geary's C	<0.001	1.506 SE=0.314 p<0.001	-0.513 SE=0.397 p=0.198	--	0.195
Sagittal	FEV1	Skewness	0.007	0.675 SE=0.111 p<0.001	0.214 SE=0.137 p=0.122	--	0.591
Sagittal	FEV1	Kurtosis	0.004	0.072 SE=0.013 p<0.001	0.021 SE=0.013 p=0.119	--	0.58
Sagittal	FEV1	FractalD	<0.001	10.081 SE=1.903 p<0.001	0.806 SE=2.246 p=0.720	--	0.572
Sagittal	FEV1	Moran's I	<0.001	-7.054 SE=1.891 p<0.001	4.403 SE=2.463 p=0.076	--	0.539
Sagittal	FEV1	Geary's C	<0.001	10.629 SE=2.216 p<0.001	-0.481 SE=2.015 p=0.812	--	0.554

Sagittal	FVC	Skewness	0.036	0.757 SE=0.136 p<0.001	0.320 SE=0.169 p=0.060	--	0.62
Sagittal	FVC	Kurtosis	0.037	0.078 SE=0.016 p<0.001	0.033 SE=0.016 p=0.043	--	0.608
Sagittal	FVC	FractalD	0.017	8.980 SE=2.414 p<0.001	1.149 SE=2.849 p=0.687	--	0.575
Sagittal	FVC	Moran's I	0.001	-5.213 SE=2.342 p=0.028	6.842 SE=3.051 p=0.026	--	0.564
Sagittal	FVC	Geary's C	0.05	8.425 SE=2.806 p=0.003	1.258 SE=2.551 p=0.623	--	0.559
Sagittal	FEV1:FVC	Skewness	0.056	--	--	0.014 SE=0.012 p=0.227	0.063
Sagittal	FEV1:FVC	Kurtosis	0.02	0.004 SE=0.002 p=0.022	-0.001 SE=0.002 p=0.388	--	0.089
Sagittal	FEV1:FVC	FractalD	0.003	1.006 SE=0.227 p<0.001	0.070 SE=0.268 p=0.796	--	0.168
Sagittal	FEV1:FVC	Moran's I	0.014	-1.056 SE=0.216 p<0.001	-0.206 SE=0.281 p=0.466	--	0.186
Sagittal	FEV1:FVC	Geary's C	<0.001	1.305 SE=0.252 p<0.001	-0.378 SE=0.229 p=0.101	--	0.221

LEGENDS FOR ILLUSTRATIONS

Figure E1. Mean radiomic features throughout the lung for sarcoidosis and healthy controls. Shaded bars represent 95% confidence bands; individual lines represent raw radiomic features throughout the lung per individual, colored by disease group. Results are shown for the right lung and all orientations.

Figure E2. Effect size of the absolute difference in radiomic features throughout the lung between sarcoidosis and healthy control subjects, adjusted for gender, age, and BMI. Assuming a normal approximation, values above 1.96 represent statistically significant differences at a significance level of 0.05. Results are shown for the right lung.

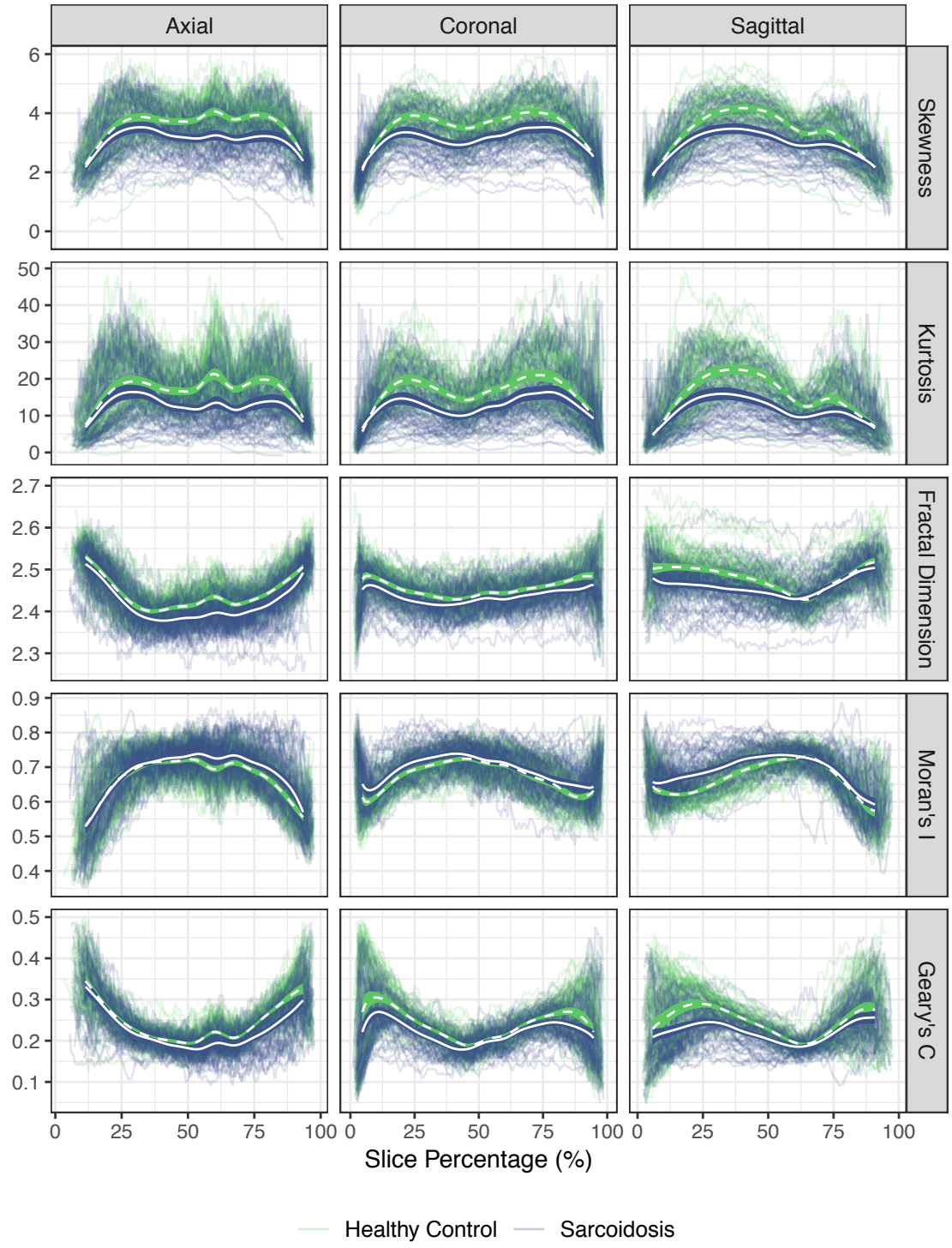
Axial
Coronal
Sagittal
Skewness
Kurtosis
Fractal Dimension
Moran's I
Geary's C
Slice Percentage (%)
Healthy Control
Sarcoidosis

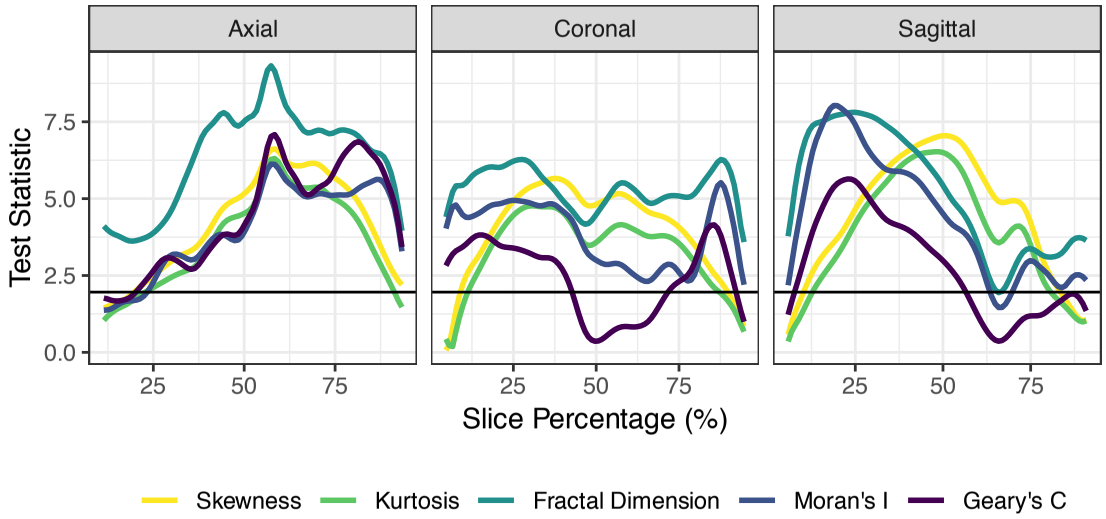
Axial
Coronal
Sagittal
Test Statistic
7.5
5.0
2.5
0.0
25
50
75
Slice Percentage (%)
Skewness
Kurtosis
Fractal Dimension
Moran's I
Geary's C